Machine learning applied to image interiors of Red-giant stars

Siddharth Dhanpal, DAA, TIFR
Advisor: Dr. Shravan Hanasoge, DAA, TIFR

July 2020

1 Introduction

All stars oscillate. These oscillations are standing waves of two kinds, one where pressure is the restoring force (p modes; like sound waves) and other where buoyancy is the restoring force creating (g modes). Studying these waves assists in understanding the structure and rotation of the Sun and other stars, with which we gain insights into processes of stellar evolution. Red giants are unique laboratories, providing a direct view of the complex death of main sequence (solar-like) stars. The seismology of red giant oscillations can be potentially used to infer the interior structure, composition, and the rotation profile. Many aspects like the angular momentum transport and evolution [1], strong magnetic fields [3], and stellar structure change in the red-giant phase[4] contain rich physics are of great interest to astrophysicists.

The *Kepler* mission (2009) has provided an enormous trove of seismic data of thousands of red giants at signal-to-noise ratios ranging from ten to ten thousand [5]. Kepler provides "light curves" for almost 200,000 stars, which are time series of minute fluctuations in their luminosities. Power spectra (squared absolute values of Fourier transforms of these recorded time series) show a sequence of peaks rising above a noisy background. The primary challenge is to label the peaks (using quantum numbers $\{n, \ell, m\}$), enabling the classification of p and g modes, rotation rates of the core and outer envelope and making precision seismology of the interior possible. Simple relationships govern the spacings[6][7] between consecutive peaks of p and g modes but mode identification is complicated by the mixed-mode behaviour that red giants exhibit. Currently Bayesian methods are applied to analyse the spectra - these are difficult to extend to the red-giant spectra[8] and only a machine learning algorithm can potentially overcome these challenges.

2 Stellar Oscillations

2.1 p modes

p modes are waves for which pressure is the restoring force (acoustic modes). These waves are the most dominant modes of the oscillation in solar-like stars, e.g., the well known 5-minute oscillations of the Sun.

$$\nu_{n\ell} \simeq \Delta\nu \left(n + \frac{\ell}{2} + \epsilon_p \right) - \ell(\ell+1) D_0 \tag{1}$$

where $\Delta\nu$ is the *large frequency separation*, D_0 is the *small frequency separation* and ϵ_p is the offset parameter. Here, $D_0 \ll \Delta\nu$.

From the expressions of $\nu_{n\ell}$, having the modes with the same value of $n + \ell/2$ have nearly same frequencies and are nearly degenerate, i.e.,

$$\nu_{n\ell} \simeq \nu_{n-1\ell+2} \tag{2}$$

Interesting characteristics of p modes are:

- All frequency peaks (resonances) of p modes which have same degree ℓ are approximately spaced uniformly apart by $\Delta\nu$.
- The peaks of $\ell = 0$ and $\ell = 2$ modes are in close proximity. These peaks are spaced by $6D_0$ which can be explained using equation 1. Similarly, the peaks of $\ell = 1$ and $\ell = 3$ are closely spaced.

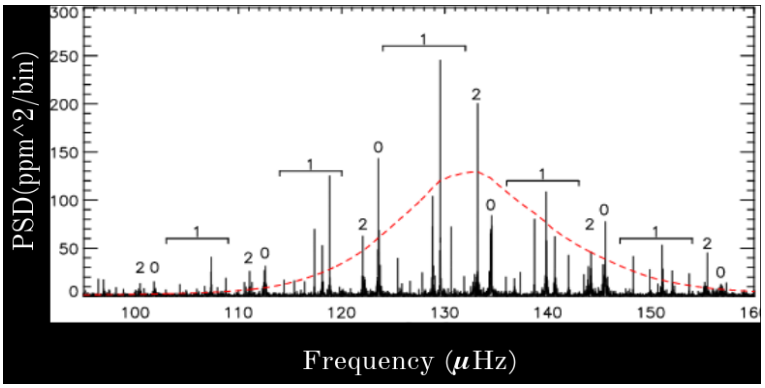

Figure 1: This figure shows the oscillation spectrum of a red giant star KIC 9145955. Here, $\ell = 0, 2$ frequency resonances are the p modes and $\ell = 1$ resonances are mixed modes of oscillation

2.2 g modes

As the name indicates, g modes are internal gravity waves which are driven by buoyancy, and therefore by gravity. Although they have not been observed directly in the sun, there have been many weak detections of g modes.

Interesting characteristics of g modes:

- All the periods of g modes with same degree ℓ are asymptotically uniformly spaced apart by $\Delta\Pi$ i.e., g mode periods $2\pi/\nu_{g_{n,l}}$ are equally separated by $\Delta\Pi$.
- For the Sun, these modes are present in the radiative core. The parameter Π_0 provides the scale of radiative core size.

2.3 Mixed p/g modes

When stars reach the end of main-sequence in the evolution, there is an increase in density gradient. One of the consequence is that a mode can be trapped in two different regions where it is a p mode in one region and g mode in other region. This mode exhibits the characteristics of both modes for the same eigenfrequency and is hence called mixed mode. Therefore, this mode is oscillatory in two different regions with different characteristic. The presence of mixed modes is evident in figure 1. The frequencies of the mixed modes asymptotically are given by solutions of equation:

$$\tan \pi \frac{\nu - \nu_p}{\Delta\nu} = q \tan \frac{\pi}{\Delta\Pi} \left(\frac{1}{\nu} - \frac{1}{\nu_g} \right) \quad , \tag{3}$$

where q is the coupling factor[12]. Here,

$$\nu_p \simeq \Delta\nu \left(n_p + \frac{1}{2} + \epsilon_p \right) - 2D_0 \ \text{ and } \ \frac{1}{\nu_g} = (-n_g + \epsilon_g)\, \Delta\Pi \tag{4}$$

2.4 Effect of Rotation

Rotation breaks the spherical symmetry of the star and lifts the degeneracy of modes in m. Slow rotation, like as Sun (450nhz) may be treated as a perturbation to the non-rotating case [11]. Each mode of degree ℓ is split into $2\ell + 1$ m components. Each mode $\nu_{n,\ell,m}$ is given by $\nu_{n,\ell,m} = \nu_{n,\ell} + \delta\nu_{n,\ell,m}$. Assuming that the star exhibits solid body rotation at rate Ω,

$$\delta\nu_{n,\ell,m} = m\,(C_{n,\ell} - 1)\,\Omega \tag{5}$$

For p modes, $C_{n,\ell} \approx 0$ and for g modes, $C_{n,\ell} \approx 1/\ell(\ell+1)$. Therefore, the multiplets of p modes are given by

$$\nu_{n,\ell,m} = \nu_{n,\ell} - m\nu_s \tag{6}$$

where $\nu_s = \Omega/2\pi$ is called the splitting. If Ω changes with radius, splitting changes as a function of the depth that the mode probes. Due to the presence of mixed modes in the evolved stars like red-giants and sub-giants, the core rotation rate can be inferred as well.

$\ell = 0, 1, 2$ modes are effected differently due to rotation in red giants. The effect is as follows:

- Effect of rotation on $\ell = 0$: No effect.
- As $\ell = 2$ is the p mode and is influenced by envelope, the effect of rotation splits each mode into 5 different modes ($m = -2, -1, 0, 1, 2$) and the frequencies of $\ell = 2$ modes are given by:

$$\nu_{n,\ell=2,m} = \nu_{n,\ell} - m\frac{\Omega_{env}}{2\pi} \tag{7}$$

- As $\ell = 1$ is the mixed mode, it is influenced by both the core (g- modes) and the envelope (p-modes). The effect of rotation splits each mode of $\ell = 1$ into 3 different modes ($m = -1, 0, 1$) and the splitting is weighted average of p-nature and g-nature in the mixed mode. The frequencies are given by:

$$\nu_{n,\ell=1,m} = \nu_{n,\ell} - m\,\delta\nu_{\rm rot} \tag{8}$$

Here, the splitting of each mixed mode frequency of value ν is given by

$$\delta\nu_{\rm rot} = -\frac{1}{2}\frac{\Omega_{core}}{2\pi}\zeta + \frac{\Omega_{env}}{2\pi}(1-\zeta) \tag{9}$$

where $\zeta(\nu)$ is in terms of ν_p and ν_g (equation (4))and given by [6]

$$\zeta(\nu) = \left[1 + \frac{1}{q}\frac{\nu^2\Delta\Pi}{q\,\Delta\nu}\frac{\cos^2\pi\frac{1}{\Delta\Pi}\left(\frac{1}{\nu}-\frac{1}{\nu_g}\right)}{\cos^2\pi\frac{\nu-\nu_p}{\Delta\nu}}\right]^{-1} \tag{10}$$

The typical variation of splitting with mixed mode frequency is shown in the 12b for a red giant KIC 5556743. The variation of splitting is discussed further in the following subsections.

2.5 Visibility of different modes and effect of inclination angle ι.

Mode Visibility: In the case of distant stars with low spatial resolutions, we observe only low degree (ℓ) modes. The visibility of a fluctuation, for a mode $f_{n,\ell,m} = AY_\ell^m(\theta,\phi)$ is given by

$$a_{n,\ell,m} = r_{\ell,m}(\iota)V_\ell A, \tag{11}$$

where V_ℓ is the mode visibility, $r_{\ell,m}(\iota)$ is the relative amplitude of the mode depends on the inclination angle ι. The visibility function depends on the limb-darkening function (star type) and the measurement technique used.

The visibility function V_ℓ is in decreases with increasing degree ℓ. Therefore, we dominantly observe only $\ell = 0, 1$ and 2 modes in the ateroseismic data as the amplitude decreases for other degree modes. We rarely observe $\ell = 3$ modes. But, $\ell = 1$ mode has higher visibility compared to $\ell = 0$ mode.

The relative amplitude is given by the following equation.

$$r^2_{\ell,m}(\iota) = \frac{(\ell-|m|)!}{(\ell+|m|)!}\left[P_\ell^{|m|}(\cos\iota)\right]^2 \tag{12}$$

where $P_\ell^{|m|}$ is the associated Legendre functions. Figure 2 shows the variation of the relative amplitudes ($\ell = 1, 2$ modes) with ι. It can be observed from the figure 2 that at $\iota = 0°$, only $m = 0$ components are visible. Therefore, it is not possible to extract information regarding rotation. For stars observed on $\iota = 90°$, components with even $\ell + m$ are observed.

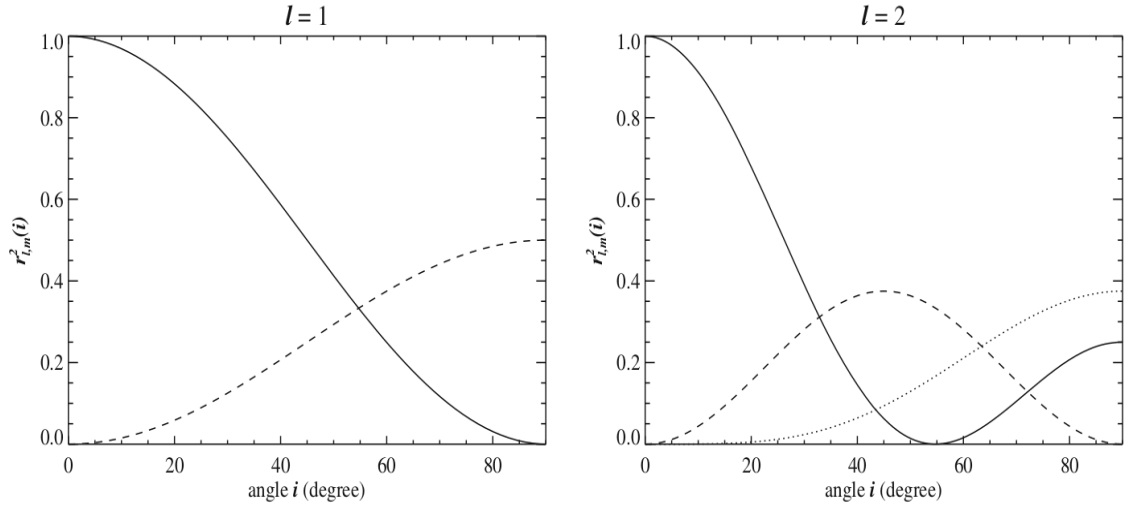

Figure 2: Relative power $r^2_{\ell,m}$ of modes in a multiplet as a function of inclination angle ι for $\ell = 1$(left) and $\ell = 2$(right). Solid,dashed and dotted lines correspond to $|m| = 0, 1$ and 2 respectively.

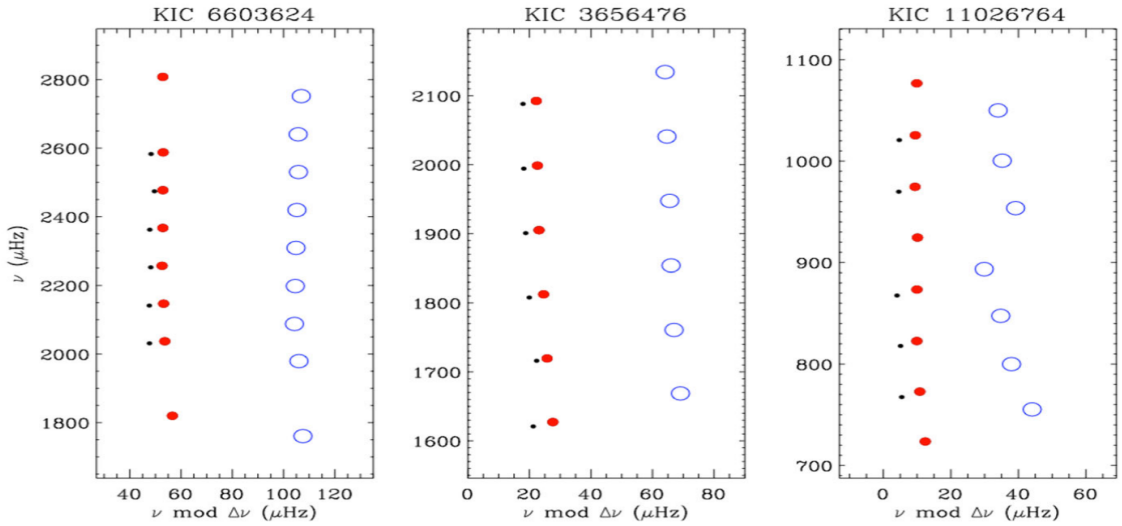

Figure 3: Echelle diagram of 3 stars observed by Kepler [11]. Three ridges here are $\ell = 0$ (filled red symbols), $\ell = 1$ (open blue symbols) and $\ell = 2$ (small black symbols). We don't observe $\ell = 3$ mode due to low visibility and the bump in the right most star indicates a mixed mode.)

2.6 Spectral Analysis

Traditional methods of analysing the spectra use Echelle diagrams. The Echelle diagram is constructed by cutting the spectrum in parts of size $\Delta\nu$ and piling these parts one on top of next. Following the first order asymptotic theory of stellar oscillations, we see the ridges of $\ell = 2, 0, 1, 3$ in an order as in figure 3. But in evolved stars, $\ell = 1$ modes aren't aligned in a straight ridge due to mixed mode as in figure 3(c).

These spectra are fitted using Bayesian analysis, assuming a background model of the spectra that depends on frequencies, splitting, inclination etc. Algorithms like Monte Carlo Markov Chain are used to find the best fitting parameters of the spectra. Some of these parameters can be correlated to each other like inclination and splitting (rotation). Hence, estimating one parameter can effect the estimate and errors of other parameters.

In order to describe the whole spectrum, a minimal set of parameters { $\Delta\nu$, ϵ_p, D_0, $\Delta\Pi$, q, ϵ_g, Ω_{env}, Ω_{core}} need to be determined:

- Learning $\Delta\nu$, ϵ_p and D_0 locates p modes in the spectrum. Similarly, locating p-modes determines $\Delta\nu$, ϵ_p and D_0.

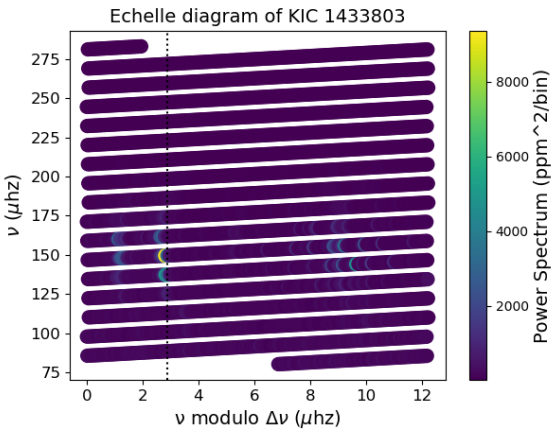

(a) Echelle diagram

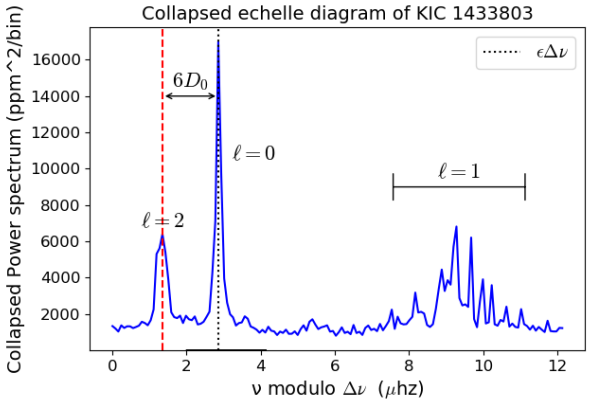

(b) Collapsed Echelle diagram

Figure 4: Figure (a) shows the echelle diagram of the star KIC 1433803. The color indicates the value of power spectrum at (ν modulo $\Delta\nu$,ν). The black dotted line is $x = \epsilon_p\Delta\nu$, which indicates all the $\ell = 0$ frequencies are lined up. Figure (b) is the collapsed echelle diagram, where the black dotted line indicates $\ell = 0$ peaks and red dashed line indicates $\ell = 2$ frequencies. The modes on the right hand side of the image are $\ell = 1$ modes. The distance between $\ell = 0$ and $\ell = 2$ peaks is given by $6D_0$

- Learning $\Delta\Pi$, q and ϵ_g locates *mixed* modes in the spectrum. Similarly, locating *mixed*-modes determines $\Delta\Pi$, ϵ_g and q.
- Learning Ω_{env} and Ω_{core} locates the rotational splitting of the p-modes and *mixed* modes. Similarly, locating rotationally split modes determines Ω_{env} and Ω_{core}.

In this project, we have used Machine learning to determine { $\Delta\nu$, $\Delta\Pi$, q, ϵ_g, Ω_{env}, Ω_{core}} which is discussed in next section. We used the echelle diagram to determine ϵ_p and D_0.

Technique to determine ϵ_p and D_0:

- After learning $\Delta\nu$ from the machine, we can construct echelle diagram as in figure 4a.
- We collapse the echelle diagram by summing up all the values of power spectrum which have same value of [ν modulo $\Delta\nu$] i.e., collapsing the echelle diagram on its x-axis. An example of a collapsed echelle diagram is shown in figure 4b
- The largest peak in the collapsed echelle diagram is due to $\ell = 0$ frequencies. This peak is located at $\epsilon_p\Delta\nu$. The closest peak to $\ell = 0$ peak in the collapsed echelle diagram is due to $\ell = 2$ ridge. Determining location of $\ell = 0$ and $\ell = 2$ peaks in collapsed echelle diagram, gives $6D_0$.

3 Convolutional Neural Network (CNN)

Artificial neural networks are inspired by and modelled on biological counterparts. Artificial neurons are functions that take inputs from prior layers, outputting a function of the sum of weighted inputs. These functions may be linear but are generally non-linear, e.g. tanh, sigmoid, reLU etc [17][19]. Neurons have weights and biases as parameters of the function, which are learned from the given data and optimized to fit the data. In a traditional algorithm, inputs and rules are provided to obtain the output. Whereas, in a machine learning algorithm, you use input and output data to obtain rules such that the neural network fits existing data and works equally well on unseen inputs. This way, an artificial neural network learns to predict the output from the training examples.

The celebrated CNN is a deep neural network that uses the convolution as a mathematical operation in one of the layers of neural network [17][18]. These networks have a wide range of applications, e.g., image and video recognition, natural language processing, image classification etc.

The different components of CNN are